Atmosphere-Ocean
Publication details, including instructions for authors and subscription information:
http://www.tandfonline.com/loi/tato20

Mesoscale wind climate modelling in steep mountains

Jean-Paul Pinard [a] , Robert Benoit [b] & John D. Wilson [c]

[a] Department of Earth and Atmospheric Sciences , University of Alberta , Edmonton, AB E-mail:

[b] Recherche en Prévision Numérique (RPN), , Environment Canada , Dorval, QC

[c] École de Technologie Supérieure de Montréal (ETS)

Published online: 21 Nov 2010.

To cite this article: Jean-Paul Pinard , Robert Benoit & John D. Wilson (2009) Mesoscale wind climate modelling in steep mountains, Atmosphere-Ocean, 47:1, 63-78, DOI: 10.3137/AO922.2009

To link to this article: http://dx.doi.org/10.3137/AO922.2009

Mesoscale Wind Climate Modelling in Steep Mountains

Jean-Paul Pinard[1,*], Robert Benoit[2,3] and John D. Wilson[1]

[1]*Department of Earth and Atmospheric Sciences*
University of Alberta, Edmonton AB
[2]*Recherche en Prévision Numérique (RPN), Environment Canada, Dorval QC*
[3]*École de Technologie Supérieure de Montréal (ETS)*

[Original manuscript received 9 October 2007; accepted 30 September 2008]

ABSTRACT *Although the Mesoscale Community Compressible (MC2) model successfully reproduces the wind climate (for wind energy development purposes) of the Gaspé region, equivalent simulations for the steep mountainous southern Yukon have been unsatisfactory. An important part of the problem lies in the provision of suitable boundary conditions in the lower troposphere. This paper will describe an alternative provision of boundary conditions to the MC2 model based partly on standard National Centers for Environmental Prediction/National Center for Atmospheric Research (NCEP/NCAR) Reanalysis statistics, however, with modified lower tropospheric conditions based on local radiosonde measurements.*

The MC2 model is part of the AnemoScope wind energy simulation toolkit which applies statistical-dynamical downscaling of basic large-scale weather situations (i.e., the NCEP/NCAR Reanalysis) to simulate the steady-state wind climate of a complex region. A case study summarized here imposes a typical mean winter temperature inversion on the boundary conditions to reduce downward momentum transfer in the MC2 model over the Whitehorse region. In conjunction with this step, the geostrophic wind at the boundaries is held constant (with height) in speed and direction, based on the (observed) dominant southwesterly winds above the mountaintops. The resulting simulation produces wind directions within the modelled domain that are in much better agreement with the available measurements. However, despite the imposed atmospheric stability, downward transfer of horizontal momentum from aloft still appears to exceed that occurring in nature.

It is recommended that (in future studies of this type regarding mountain wind climate) the input statistics processed from the NCEP/NCAR Reanalysis be modified by referencing the geostrophic winds to a level above the mountaintops. It is also suggested that converting to a height (z) coordinate system may reduce the erroneous downward momentum transfer found in the present terrain-following grid.

RÉSUMÉ *[Traduit par la rédaction] Même si le modèle de mésoéchelle compressible communautaire (MC2) reproduit adéquatement la climatologie du vent (pour les besoins du développement éolien) dans la région de Gaspé, il n'y est pas parvenu de façon satisfaisante lors de simulations équivalentes dans les régions de montagnes escarpées du sud du Yukon. Une partie importante du problème réside dans la fourniture de conditions aux limites appropriées dans la basse troposphère. Cet article décrira une autre façon de fournir des conditions aux limites du modèle MC2 fondée en partie sur les statistiques normalisées des réanalyses des NCEP/NCAR (National Centers for Environmental Prediction/National Center for Atmospheric Research) avec, cependant, des conditions modifiées dans la basse troposphère en fonction des mesures locales obtenues par radiosondes.*

Le modèle MC2 fait partie de la trousse de simulation de l'énergie éolienne AnemoScope qui applique une réduction d'échelle statistique-dynamique à des situations météorologiques à grande échelle (c.-à-d. les réanalyses des NCEP/NCAR) pour simuler la climatologie du vent en régime permanent dans une région au relief accidenté. Une étude de cas que l'on résume ici impose une inversion thermique moyenne caractéristique de l'hiver comme conditions aux limites pour réduire le transfert de quantité de mouvement vers le bas dans le modèle MC2 au-dessus de la région de Whitehorse. En même temps, le vent géostrophique aux limites est maintenu constant (avec la hauteur) en vitesse et en direction et basé sur les vents dominants du sud-ouest (observés) au-dessus du sommet des montagnes. La simulation résultante produit des directions du vent dans le domaine modélisé qui s'accordent beaucoup mieux avec les mesures que nous avons. Cependant, malgré la stabilité atmosphérique imposée, le transfert de quantité de mouvement vers le bas à partir des couches en altitude semble encore plus important que dans la réalité.

Nous recommandons que (dans les futures études de ce genre sur la climatologie du vent en régions montagneuses) les statistiques dérivées des réanalyses des NCEP/NCAR fournies en entrée soient modifiées en définissant les vents géostrophiques par rapport à un niveau situé au-dessus du sommet des montagnes. Nous pensons aussi que l'emploi d'un système de coordonnées de hauteur (z) pourrait réduire le transfert erroné de quantité de mouvement vers le bas observé avec la grille actuelle, qui épouse le relief.

*Corresponding author's e-mail: jpinard@ualberta.ca

1 Introduction

A wind energy project is being considered for the mountainous Whitehorse region to complement the existing hydroelectric system to meet the Yukon's growing energy demand. In this paper we present the results of the simulation of the long-term mean annual wind energy climate over the Whitehorse mountainous region (see Fig. 1), using the statistical-dynamical downscaling approach to extract a high resolution local climate from the observed larger scale wind climatology. As the primary component of the wind energy simulation toolkit AnemoScope (developed by Recherche en Prévision Numérique, Environment Canada), the Mesoscale Compressible Community (MC2) model is used in the EOLE (or diagnostic) mode over high-resolution topography to provide a wind field that is in equilibrium with the boundary conditions derived from large-scale climate. These boundary conditions will be of crucial importance, and their optimization is the topic of this paper.

The standard procedure has been to set the boundary state using the mean geostrophic winds and temperatures defined by the National Centers for Environmental Prediction/National Center for Atmospheric Research (NCEP/NCAR) Reanalysis (Reanalysis hereafter; see Section 3 for a full description); hundreds of such macroscopic climate states have been extracted from 43 years of global measurements (Kalnay et al., 1996). For any region of interest, the MC2 model is run to steady state for each of the relevant boundary states. (If desired, each MC2 solution can be further refined on even higher resolution terrain, using a microscale simulation tool; however, this is not relevant to the present work.)

In Yu et al. (2006) the toolkit was used to simulate the wind climate in the Gaspé region of Quebec, where more than 90% of the surface has an elevation lower than 1000 m above sea level (ASL). The resulting simulations produced near-surface winds that were in general agreement with the observations. However, when used by Pinard et al. (2005) to simulate winds over the southern Yukon, where the terrain relief ranges from 600 m to more than 3000 m ASL, a similar approach resulted in erroneous long-term mean surface wind directions in some major valleys and on nearby ranges: it was apparent that in the simulation, winds aloft had tended to mix down into the valleys, resulting in this unrealistic long-term climatology.

A study of radiosonde temperature profiles from the Whitehorse upper-air station (Pinard, 2007) made it clear that the temperature inversion is a dominant feature and must play an important role in decoupling valley air from the winds aloft. In the absence of strong downward momentum transport, the pressure gradient is the main forcing mechanism in the channelled valley flow (e.g., Vogel et al., 1986; Gross and Wippermann; 1987; Smedman and Bergström, 1995; Bergström and Juuso, 2006). In view of this forcing mechanism, one avenue available to improve the high-resolution wind climate simulation would appear to be the provision of driving (boundary) states that are more strongly stratified. This is justifiable because the (true) long-term annual wind climate is certainly more heavily weighted by the strong wintertime winds than it is by winds during the other (less strongly stratified) seasons.

The Reanalysis is universally available for mesoscale modelling and it is important to find ways to improve the way it is used to provide the boundary conditions for the MC2 model and the AnemoScope toolkit. The form in which the Reanalysis has been used has produced rather weak lapse rates in the lowest portion of the model domain. In Fig. 8 of Pinard et al. (2005), for example, the temperature lapse rates in the lowest 1500 m for the dominant winter profiles (bins) are approximately –6°C km^{-1} (potential temperature lapse rate of +4°C km^{-1} in Fig. 8) compared to the much stronger temperature inversions of +8°C km^{-1} measured by radiosondes at the Whitehorse station. Our objective is to show that the method by which the boundary conditions are derived from the Reanalysis may need to be modified to reflect the stratified nature of the atmosphere in mountainous terrain such as the Yukon.

In the following sections we show that an improved MC2 model simulation of wind climate in the Yukon can be achieved by supplying the MC2 model with a boundary wind profile that can be taken from the upper levels of the Reanalysis (above the mountaintops, where the wind is geostrophic) but a boundary temperature profile that more closely reflects the temperatures reported by the Whitehorse upper-air observations. The altered constraining temperature profile results in altered orographic winds over the simulated terrain.

2 AnemoScope toolkit

Recherche en Prévision Numérique (RPN) of Environment Canada has developed tools to simulate wind energy in complex terrain. The latest development is AnemoScope, a PC-based wind simulation toolkit consisting of both mesoscale and microscale components. AnemoScope is the next generation of a wind climate mapping software product, the Wind Energy Simulation Toolkit (WEST) which is described in Pinard et al. (2005) and Yu et al. (2006). A user's guide to AnemoScope can be found in CHC&EC (2006). RPN has also developed the Canadian wind atlas (www.windatlas.ca) which is based on the same principles as AnemoScope, excluding the use of the microscale component. The simulation statistics (provided by the MC2 model) are available on the wind atlas website, and users of AnemoScope can produce their own microscale simulations.

AnemoScope is based on a statistical-dynamical downscaling approach (Frey-Buness et al., 1995). The assumption is that regional climate is associated with a specific frequency distribution of basic large-scale weather situations or climate bins (see Section 3). Each climate bin is characterized by its vertical profiles of horizontal wind speed, wind direction and temperature and is used to initialize (and bound) a mesoscale simulation (MC2). The winds are initially treated as geostrophic and used to set the horizontal pressure gradient at all levels in the model. In the present AnemoScope

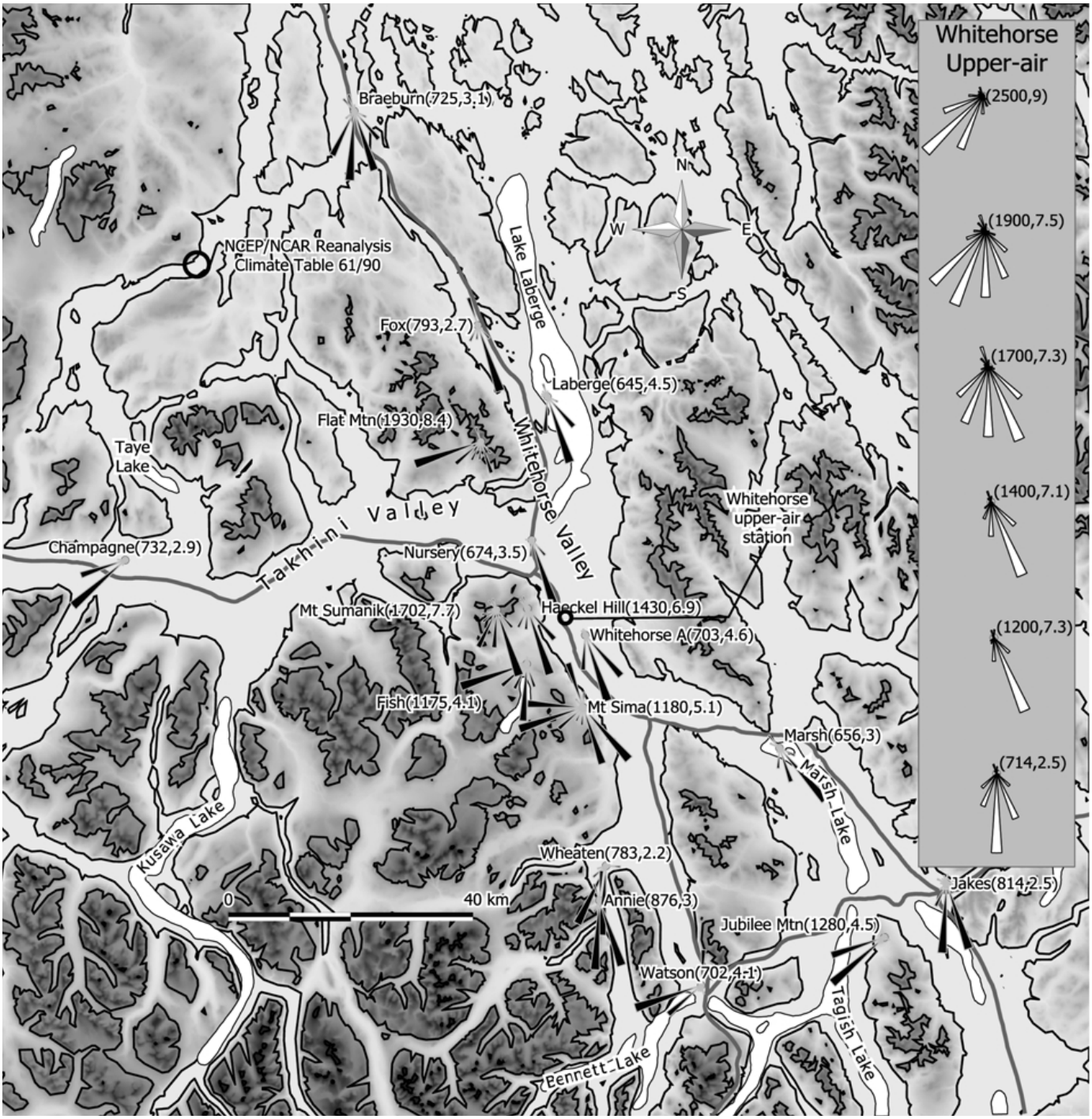

Fig. 1 Map of the south-central Yukon including the Whitehorse area, showing contour lines at 900 m and 1500 m ASL. The roads are grey. For present purposes two valleys are of most interest: the Whitehorse Valley and the Takhini River valley. The wind monitoring stations are shown along with their wind energy rose, surface elevation (m ASL), and mean annual wind speed (at 30 m AGL). The inset roses for the Whitehorse upper-air station are labelled with height (m ASL) and mean annual wind speed for the period 2001–05. The wind energy-frequency rose is calculated, for each direction, as the product of the cube of the mean wind speed and its frequency of occurrence divided by the sum of those products in all directions.

parameterization the surface-layer wind is then modified to reflect surface conditions. Topography is introduced progressively during the model run, starting from a flat plain at sea level at initial time. With the lateral boundary conditions held constant, the interior high resolution climate corresponding to each macroclimate bin is simulated by running the MC2 model for a sufficiently long time to achieve a steady state (i.e., typically 6–9 hours of physical time, as opposed to computation time). The simulation resulting for each climate bin is weighted by the frequency of occurrence of that bin to produce a bivariate frequency distribution (frequency distribution of wind by direction and wind-speed interval). The

statistical result can be interpreted on its own, or can be used to initialize a high-resolution microscale model at each mesoscale grid point. This method of initializing this mesoscale model is known as the EOLE mode of the MC2 model.

MC2 is a compressible, non-hydrostatic, limited area model (Tanguay et al., 1990; Thomas et al., 1998; Girard et al., 2005) that (in AnemoScope) is used in a diagnostic (i.e., steady state or EOLE) mode, to produce a three-dimensional atmospheric state reflecting only the specified lateral boundary conditions, topography and surface roughness: more specifically, other forcing mechanisms that would be an essential component of weather (as opposed to wind climate) prediction are excluded, e.g., surface-air energy fluxes, latent heating effects, clouds, etc. This exclusion allows the model to reach steady state efficiently and, more importantly, relieves the user of the need to provide unknown boundary values (of surface sensible heat flux density, etc.). As a consequence of the simplification, the computed equilibrium state depends mainly on temperature stratification, pressure gradient and wind speed (as controlled by the boundary profiles), on model topography and on resolution, whereas the influence of the initial state, many hours after initialization when steady state has been attained, is "forgotten". Owing to the neglected physical processes, certain mesoscale phenomena such as diabatic slope winds and land/lake breezes cannot be simulated, so that their influence is excluded from the computed long-term climatology. While these types of orographic circulations are, in and of themselves, usually too weak to produce significant wind energy, the neglected physical processes that give rise to them undoubtedly do modulate the strength of the wind; thus their neglect does, to some degree, compromise accuracy of the computed wind climate.

Because MC2 is a fully non-linear finite difference model, reduction of the horizontal grid spacing below 1 km necessitates greatly increased computer resources to deal with the rapidly increasing number of grid points and smaller time steps. To overcome this practical limitation, a microscale model, MS-Micro (see Walmsley et al., 1990) is coupled to the MC2 model output, to simulate winds at a finer resolution. Based on linearized equations of motion and a semi-analytic solution method, the MS-Micro model can simulate winds at a grid resolution of the order of tens of metres. Since this study concerns a mesoscale atmospheric flow, the MS-Micro model is not utilized here: we are trying to solve a problem present in the mesoscale part of the overall downscaling process of AnemoScope.

3 NCEP/NCAR Reanalysis extracted for driving the MC2 model

The large-scale climate classification driving the MC2 model is derived from a global 43-year (1958–2000) long-term data set provided by the Reanalysis (Kalnay et al., 1996) on a latitude-longitude grid spaced at 2.5° intervals and covering pressure levels from sea level to the 10 mb level. The procedure used by AnemoScope (i.e., to drive the MC2 model) is to extract from the Reanalysis a set of wind climate bins, classified according to the sea-level pressure gradient (which can be considered to imply a fictive sea-level geostrophic wind speed and direction) and the vertical shear of wind speed between 0 and 1500 m ASL.

There are 14 speed classes (2, 4, 6,...,30, and >34 m s^{-1}, 16 direction sectors, and two shear classes (positive or negative, shear is not significant for wind speed less than or equal to 2 m s^{-1}, resulting in (a maximum of) 432 bins at each latitude/longitude node. Each bin has its own characteristic one-dimensional atmospheric state, as defined by averaging wind speed, direction and temperature over all weather situations in the Reanalysis that conform to that bin. Each mean weather situation (bin) is interpolated to four tropospheric pressure levels (1000, 850, 700 and 500 mb), and these profiles are mapped onto the MC2 model coordinate by assuming that these mandatory levels correspond to 0, 1500, 3000 and 5500 m ASL.

In the southern Yukon, the 2.5° grid spacing implies that nodes are spaced approximately 130 km apart in the east–west direction and 275 km apart in the north–south direction. The climate table used to simulate the Whitehorse

TABLE 1. Comparison of the Reanalysis and the radiosonde observations in the Whitehorse area for the (43-year) period 1958–2000. The Whitehorse radiosonde station is at 704 m ASL at the bottom of a south–southeast oriented valley. The Reanalysis is a forty-three year mean annual climate for node 61/90 (Whitehorse region, see Fig. 1), formed as the weighted mean of the 287 bins pertaining to that node. The winds at given elevations (m ASL) are considered geostrophic for the Reanalysis. Note that the sea-level wind is fictional.

	Elevation	0 m	1500 m	3000 m	5500 m	Units
Reanalysis	Variable					
	Wind Speed	10.1	6.0	4.8	6.3	m s^{-1}
	Wind Direction	ESE	SSE	S	SSW	
	Temperature	279	269	262	246	K
	Lapse Rate	–6.7	–4.0	–6.4		K km^{-1}
	Elevation	714 m	1500 m	3000 m	5500 m	Units
Radiosondes	Variable					
	Wind Speed	2.4	6.8	9.7	13.6	m s^{-1}
	Wind Direction	SSE	SSE	SW	WSW	
	Temperature	274	271	263	247	K
	Lapse Rate	–3.8	–5.3	–6.4		K km^{-1}

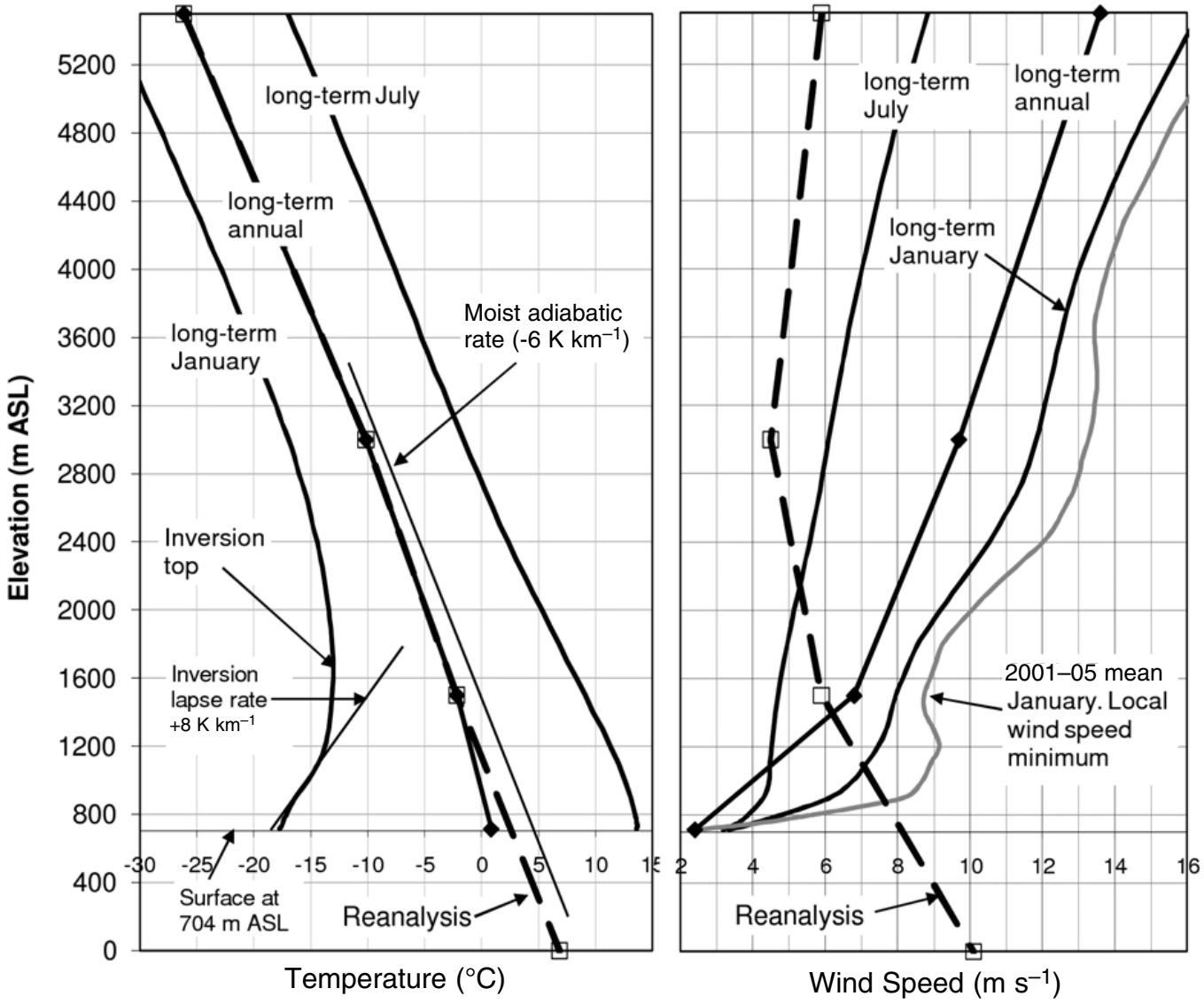

Fig. 2 Vertical profiles of temperature and wind speed for the Reanalysis and the Whitehorse radiosondes for the 43-year, 1958–2000 period. The temperature and wind speed profiles (long-term annual mean) for the Reanalysis are represented by dashed lines.

wind climate is that associated with a node (Table 61/90) located at 61.25°N and 136.25°W, about halfway between the Champagne and Braeburn observation sites (marked in Fig. 1). The climate table for this node contains 287 climate bins occurring with non-zero frequency.

4 Comparing the Reanalysis to observations

The input wind data from Table 61/90 of the Reanalysis are summarized in Table 1, along with observations from the Whitehorse radiosondes. The annual mean temperature profile according to the Reanalysis (Fig. 2) reveals a mean temperature lapse rate of –6.7 K km^{-1}, corresponding to conditionally unstable stratification. The Reanalysis lapse rates in the lowest 1500 m ASL range across the 287 climate bins from –4.5 to –9.1 K km^{-1}. The neighbouring Reanalysis nodes have characteristics that vary only slightly from this. In contrast to the Reanalysis, radiosondes indicate that the long-term annual mean temperature profile is stably stratified (i.e., the environmental lapse rate is more stable than the moist adiabatic rate of approximately –6 K km^{-1}, more strongly so toward the valley bottom (700 m ASL). Furthermore, far stronger valley inversions, with lapse rates of about +8 K km^{-1} and caps at around 1600 m ASL, dominate the Whitehorse climate during winter. The important control of these more stable temperature profiles on the long-term wind climate is not fully reflected in the mean annual temperature profile.

Figure 2 indicates that only at around 1500 m ASL are annual mean wind speeds from the Reanalysis (thick dashed line) and from the Whitehorse radiosonde of similar magnitude. At higher levels, radiosonde long-term annual mean wind speeds are much faster than those indicated by the

Reanalysis, while conversely, at lower levels radiosonde wind speeds are slower than those of the Reanalysis, which increase towards and are fastest at sea-level. (Note that the high sea-level windspeed from the Reanalysis is unrealistic and is caused by neglecting the effects of friction, i.e., divergence of the Reynolds stress tensor and of topographic steering.) Evidently then, it would be inappropriate to use the sea-level wind speed in Table 1 as a lateral boundary condition for the MC2 model.

The temperature lapse rates and wind speeds discussed here play an important role in the behaviour of wind flow in mountainous terrain. A qualitative insight into the influence of atmospheric stability and wind speed on flow over terrain may be gained by considering the Froude number, defined by

$$\mathrm{F} = \frac{U}{NH}, \tag{1}$$

where U is the mean wind speed, H the topographic amplitude, and N the Brunt-Väisälä frequency

$$N = \sqrt{\frac{|g|}{T_v}\left(\frac{\Delta T_v}{\Delta z} - \Gamma_d\right)} \tag{2}$$

where g is the gravitational acceleration, T_v the virtual temperature, and $\Gamma_d = 9.8$ K km^{-1} (the dry adiabatic lapse rate). The usefulness of F as a diagnostic index stems from the fact that its square is the ratio of the kinetic energy (per unit mass) of oncoming air to the work needing to be done (per unit mass, against gravity) to ascend over the terrain: thus, the magnitude of F loosely indicates the ability or tendency of air to ascend over terrain, as opposed to deviating along valleys and over passes. In principle, the lower the value of F the shallower the layer of air able to ascend over a barrier and, correspondingly, the deeper the underlying column of cold valley air that must deviate horizontally around a mountain obstacle. This appealing interpretation is of course complicated by the fact that, in the case of real winds over real terrain, there is likely to be ambiguity in the specification of each of the factors, U, H and N, determining F.

In a stably stratified environment, under moderate wind conditions $\mathrm{F} \lesssim 1$. For the annual mean conditions given in Table 1 the Brunt-Väisälä frequencies according to the Reanalysis and the radiosondes were $N = 0.012$ and 0.015 s^{-1}, respectively, while the corresponding Froude numbers were F = 0.5 and 0.4. Season-specific values from the radiosondes were $N_{summer} = 0.01$ s^{-1}, $N_{winter} = 0.02$ s^{-1} and $F_{summer} = 0.56$, $F_{winter} = 0.35$. Thus, across all seasons the seasonal mean temperature profile is stably stratified and valley air should be expected to have a strong tendency to move around mountain obstacles, with minimal vertical movement.

Figure 2 also gives the mean January wind speed profile for a shorter, more recent period, 2001–05. Aside from apparent long-term increase in wind speed in the Whitehorse region, what is noteworthy in this profile is the local minimum in windspeed that occurs at 1500 m ASL. Inset on Fig. 1 are wind roses calculated from the Whitehorse radiosonde. Except at 714 m ASL (where the southerly dominant wind reflects the local land forms (Pinard, 2007)), at levels below 1500 m ASL the dominant wind tracks along the valley; this trend extends to 1600 m ASL according to a mean January 2001–05 wind rose (not shown). Above 1600 m ASL the winds gradually veer to a well-defined southwesterly direction at 2600 m ASL. We tentatively suggest that the observed local minimum in radiosonde windspeed for this particular January period occurs at or below the level where a dividing streamline surface (Whiteman, 2000) separates energetic winds aloft that are able to cross the ridges from decoupled winds moving horizontally within the valley.

According to climatological geopotential height fields extracted directly from the Reanalysis (website), the annual mean free winds above the mountaintops (i.e., 3000 m ASL) of the Whitehorse region are predominantly southwesterly, if they are assumed to be geostrophic. Within the valley, elevations at or below 1500 m ASL the geopotential height fields imply that geostrophic winds would be southerly (that is, long-term climatological isobars at 1500 m ASL run north–south in the Whitehorse region, with pressure increasing towards the east), while at sea level they would be southeasterly. The wind directions from the geopotential height fields somewhat resemble those derived from the Whitehorse radiosonde that are also shown in Fig. 3 as wind-energy frequency roses (note that the measured winds at 1500 and 714 m ASL are ageostrophic, controlled by the valley orientation). The Reanalysis wind roses as derived for use in AnemoScope (following the method in Section 3) are also shown in Fig. 3, and summarized in Table 1. The Reanalysis roses indicate that the winds are more southerly than the directly derived radiosonde observations at 3000 m ASL but quite comparable with the observations at 1500 m ASL. At sea level the Reanalysis wind rose is dominated by east-southeasterly winds (note: geostrophic here) whereas the observations in the valley bottom (714 m ASL) follow the south–southeast orientation of the Whitehorse Valley.

Surface observations from nearby, well-exposed stations at various elevations compare well with the radiosonde. There are about 25 observation sites in the Whitehorse region, half of them located in the valley bottoms. In Fig. 1, most of these wind monitoring stations are shown along with their wind energy roses, ground elevation, and mean wind speed (at 30 m above ground level (AGL)). Details for the stations used in this study can be found in Pinard (2005, 2007) and Pinard et al. (2005). Long-term annual mean wind speeds at the bottom of the valleys are generally between 1 and 4 m s^{-1} (measured at 10–30 m AGL), whereas sites on mountaintops that are open to the south and west have wind speeds between 5 and 8 m s^{-1}. The wind roses in Fig. 1 indicate two important prevailing wind directions: southwest and southeast. The stations at Flat, Watson, Jubilee and Champagne measured southwest winds. The other stations measured south to southeasterly winds, depending on the local orography around each site.

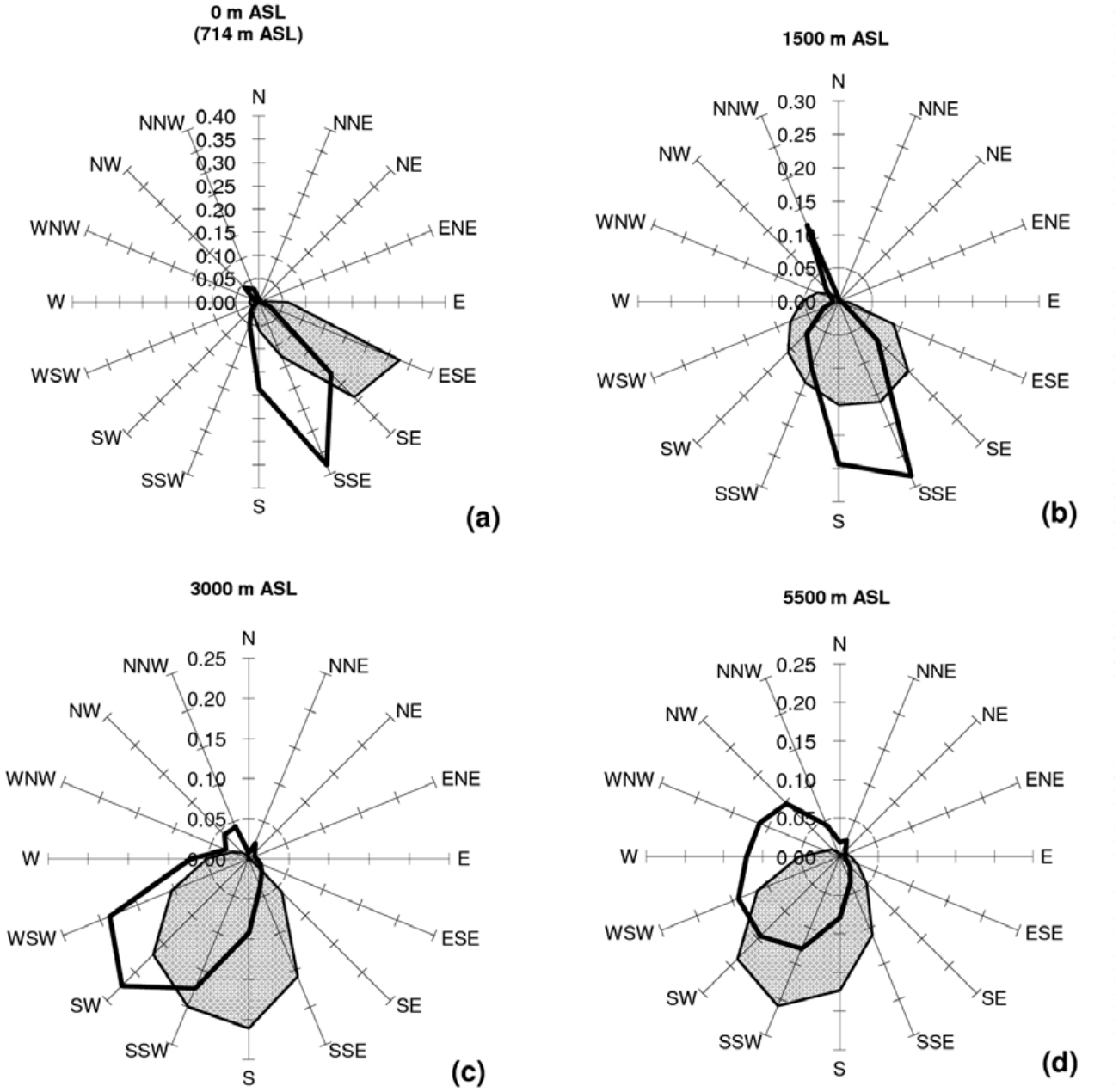

Fig. 3 Wind energy-frequency roses comparing the Reanalysis (shaded) and the Whitehorse radiosondes (outlined) at altitudes 0 (714 only for radiosondes), 1500, 3000 and 5500 m ASL. Both analyses are for the period 1958–2000. The Reanalysis roses are from node 61/90 at the location shown in Fig. 1 and are those used as input to the MC2 portion of the AnemoScope toolkit. The wind energy-frequency is calculated as the product of the percentage frequency and the cube of the mean wind for each direction, divided by the sum of those products in all directions.

In some locations the atmospheric stratification affects the dominant wind direction relative to the orography. At Mount Sima for example, the station is at mid-height on the west side of the Whitehorse Valley and has some orographic blocking from the southwest (see Fig. 1). In the summer, under rather weak stratification this station measured prevailing wind directions from the west-southwest. In the winter, however, with more stably stratified conditions, the most dominant wind was from the southeast. The Fish station to the northwest measured the same seasonal trend.

The Reanalysis (modelled) climate is most strongly influenced by observations from the nearest radiosonde station, in this case the Whitehorse station (85 km southeast of node 61/90). The southeasterly low-level winds of the Reanalysis are attributable to the Whitehorse observations having been taken within this southeasterly valley. In contrast, the Champagne station, 70 km west of Whitehorse, measured predominantly southwesterly winds. What would the Reanalysis look like for this region had the radiosonde station been located at Champagne? We raise this question not in

order to answer it but simply to highlight a logical weakness of the present approach to climate input for simulating the regional wind climate.

5 Numerical simulations

As stated earlier, defining long-term wind climate by appropriately weighting each of the MC2 model solutions driven by each of the (287) distinct climate macrostates (as defined by the Reanalysis), produced doubtful results in the mountainous regions of Whitehorse. In Pinard et al. (2005) it was not clear which of the driving climate macrostates were the dominant cause of the erroneous results. In this study we wish to simplify our simulation and so in this section we shall compare two simulated wind climates, each derived by driving the MC2 model with a simple, *single*, mean macroclimate:

- climate macrostate Ω_1: weighted average wind speed and temperature of the 287 Reanalysis bins and wind directions based, partly, on the wind energy-frequency roses shown in Fig. 3
- climate macrostate Ω_2: wind speed and direction taken as constant with height and approximately equal to the Reanalysis winds (averaged over all 287 bins) above mountain tops; temperature profile representative of winter conditions as measured by the Whitehorse radiosonde.

Both simulations use the same 450 × 450 km domain with a 5 km grid resolution and use the surface elevation and land use data from the 1 km database of United States Geological Survey (USGS) (the elevated terrain is blended into a bordering sea-level flat plain at the boundaries). The parameters used for the MC2 simulations are listed in Table 2. The vertical resolution is such that the lowest grid level (for horizontal components *U* and *V*) is 40 m above the surface (or AGL), with the next highest gridpoints at 125 and 220 m AGL and with a gradually increasing interval thereafter. The land use data are converted to surface roughness using a look-up table (see Pinard et al. (2005)). Typically, the higher elevations in the land model are classified as tundra, with surface roughness z_o = 0.01 m. Valley bottoms are mainly covered with spruce forest, represented by z_o = 1.5 m. Lakes are assigned z_o = 0.001 m.

TABLE 2. List of parameters used in the simulations of MC2.

Parameter descriptions	Values	Units
Horizontal resolution	5	km
Horizontal grid	90 × 90	grid cells
Height of model lid	20	km
Number of vertical levels	35	
Number of levels in 1500-m boundary layer	12	
Blending zone between mountains and flat plain	8	grid cells
Width of flat plain around model	9	grid cells
Time step	60	seconds
Total steps	960	
Total model time	16	hours
Time for mountain growth	4.2	hours
Run time on modern computer	<1	hour

a *Climate Macrostate* Ω_1

This macrostate is defined by averaging over the 287 Reanalysis bins (Table 61/90) representing the Whitehorse area climate, and is given in Table 3. The (scalar) mean wind speed (temperature) at each level is the sum of the frequency of occurrence in each bin multiplied by the associated wind speed (temperature). The wind directions listed in Table 3 veer from southeast at sea level to southwest at 5500 m ASL and these reflect the prevailing wind directions indicated in the wind energy roses of Fig. 3. The veering of wind directions in this single profile is quite comparable to individual climate profiles of the most important (i.e., most frequent) bins in climate Table 61/90. As is standard procedure in AnemoScope, the sea level winds are reduced by 40% and rotated by 45° counter-clockwise[1], but note that the surface *pressure gradient* of the Reanalysis is not altered. The temperature profile in the lowest 1500 m represents a mean temperature lapse rate of –6.7 K km^{-1}.

The resulting MC2 simulation driven by climate macrostate Ω_1 is shown in the form of surface horizontal winds in Fig. 4. The simulated wind vector field of the present single MC2 model run is comparable to that which results from averaging all 287 MC2 model runs, one for each climate bin (both results showed similar wind directions along the boundary, within the valleys and at the mountaintops). Along the boundaries (not shown in the figure) and on the flat plain (at 0 m ASL) surrounding the model terrain, the winds are easterly, that is, they are in conformance with the boundary condition with its rotated surface wind direction (i.e., 135 – 45 = 90°; as stated earlier, the angle adjustment is made after the pressure gradient is set for the initial and

[1]In the model's low lying regions, surface and orographic roughness does not adequately reduce and rotate the sea-level geostrophic winds of the Reanalysis to reflect actual, or boundary layer winds. This results in a surface wind that is too fast and that blows from a direction that is approximately 45° in error. While this adjustment has a significant effect on the simulation of winds over low terrain, the rotation becomes less important in mountainous regions — as will become evident.

TABLE 3. Input parameters of the climate macrostate Ω_1 representing the Reanalysis. This macrostate is used in the MC2 simulation of the Whitehorse area.

	0 m	1500 m	3000 m	5500 m	Units
Speed	10.1 × 0.6	6.0	4.8	6.3	m s^{-1}
Direction	135 – 45 = 90	158	180	223	degrees
Temperature	279	269	262	246	K
Lapse Rate	–6.7	–4.0	–6.4		K km^{-1}

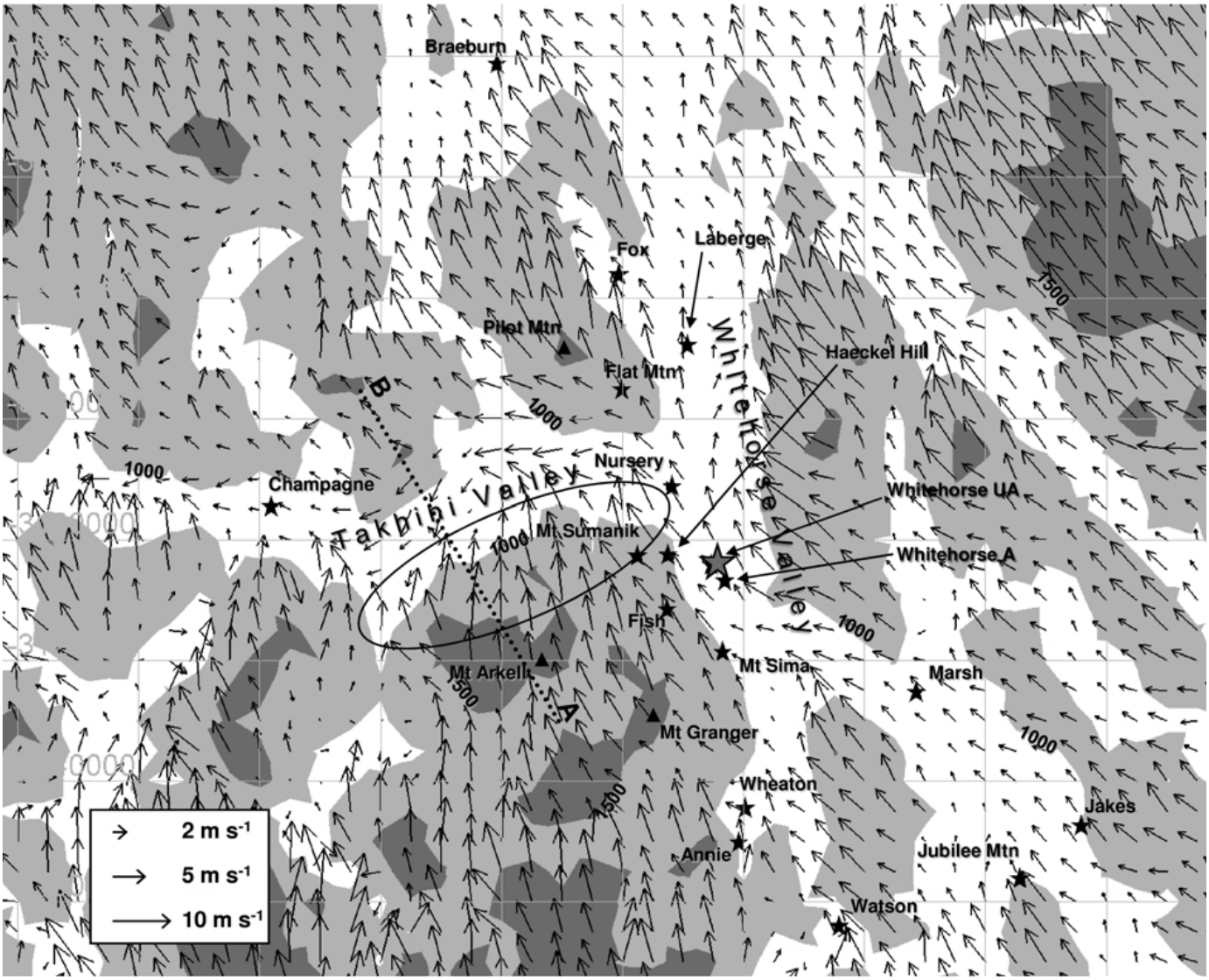

Fig. 4 Outcome of wind climate simulation based on driving MC2 with climate macrostate Ω_1, which represents the Reanalysis. The vectors are long-term mean near-surface (40 m AGL) winds in m s^{-1}. There are two elevation contours at 1000 and 1500 m ASL; the distance between two grid points (tail of each arrow) is 5 km.

boundary conditions). Note that a second simulation was made without the 45-degree rotation of the surface winds and resulted in southeasterly winds along the boundaries but with little alteration of the diagnosed surface winds in the interior of the domain.

In the central portion of the domain, within northwest-southeast oriented valleys such as the Whitehorse Valley, the simulation from macrostate Ω_1 correctly simulates southeasterly winds (compare Figs 1 and 4). But the similarity with the observations ends there. Outside of the Whitehorse Valley, the surface winds over the rest of the terrain are also predominantly southeasterly with easterly and southerly components, contradicting most of the observations. In the Takhini Valley for example, the simulated winds are easterly (Fig. 4), and in some places northeasterly — in contrast with the dominant southwesterly winds measured by the Champagne surface station. On the mountaintops, the simulated winds are southeasterly, at odds (by some 90°) with the southwest winds measured by the Flat Mountain surface station and the radiosonde at 1900 m ASL. It should be noted that the simulated southeasterly winds at the mountaintops conform to the initial and boundary wind directions that were imposed on the simulation (as noted in Table 3), being 158° at 1500 m ASL. At 700 mb in the model (approximately 3000 m ASL, not shown) the simulated winds are southerly, consistent with the boundary conditions given by the Reanalysis at the same elevation but not consistent with the radiosondes, which measured predominant southwesterly winds.

Another important group of unrealistic modelled wind vectors that should be noted are the strong southeasterly winds that appear on the north-facing slopes of the Takhini Valley (see oval in Fig. 4). These large magnitude surface winds appear from the mountaintop (approximately 1700 m ASL) down to 800 m ASL on the lee side of the mountain. Several

hundred metres below the peak these winds have speeds that are double those determined at the crest. The wind flow pattern can be better visualized with a vertical cross-section of the potential temperature and vertical wind speed across the Takhini Valley. As shown in Fig. 5, the isentropes and isotachs reveal significant sinking motion reaching a magnitude of 0.35 m s^{-1} down into the Takhini Valley, especially near the surface. However, observations of the mean state of the Yukon climate (see Pinard, 2007) suggest these cross-valley winds on lee slopes are unusual — winds typically flow horizontally around mountains, and there appears to be little vertical motion, especially during the winter months. These problematic strong lee-slope winds were also simulated by Pinard et al. (2005) in the deep Kluane Valley, west of Whitehorse, and these also contradicted the surface observations in this valley. It had not been clear at the time which climate macrostate was causing this problem.

How might one improve on this, the Ω_1 simulation? Ω_1 was initialized with a southeasterly (geostrophic) wind in the lower troposphere (i.e., Fig. 3b), in light of which (and considering the improperly imposed easterly surface wind) the successfully simulated southeast wind in the Whitehorse Valley is unsurprising. We note, though, that corresponding to the southeast geostrophic wind the alignment of the isobars implies the simulation must have come to equilibrium with a pressure gradient oriented southwest–northeast, i.e., with higher pressure to the northeast (which is, in fact, the case in the simulation). Since the Takhini Valley is oriented west–east, it is reasonable to infer that this background macroscopic pressure gradient has driven the (simulated, and false) easterly winds in that valley, winds whose orientation is at odds with the wind direction from observations. If the background pressure gradient were rotated so that higher pressure lay to the southeast, one would then expect southeast ageostrophic winds in the Whitehorse Valley, but the corresponding southwesterly geostrophic wind in the lower troposphere would be compatible with observations aloft. It also seems advisable to reduce or eliminate the noted spurious downward mixing associated with the Ω_1 macrostate, for which N = 0.01 s^{-1} and F = 0.6, assuming a characteristic mountain height of 1000 m and wind speed of 6 m s^{-1}. The effective Froude Number can be reduced by strengthening the stratification (increasing N), which should reduce the downward transfer of momentum into the valleys.

In view of the above-noted problems with the MC2 wind simulation when driven by climate macrostate Ω_1, in the next subsection we introduce driving macroclimate Ω_2 which results in improved agreement of the modelled and observed wind climates.

2 *Climate Macrostate* Ω_2

Although the Reanalysis indicates that at lower elevations (≤1500 m ASL) the geostrophic sea level winds are from the southeast, let us instead assume that the low-level geostrophic winds are aligned with the southwest winds that occur above the mountaintops — in effect, we consider the Reanalysis data for the air aloft to be more reliable than the data for the layer between mountaintop and sea level. For simplicity, let us also define a height-independent wind speed that is comparable to that of the Reanalysis above the mountaintops. The lower boundary layer attenuation and rotation of the wind vector are not applied in this simulation. See Table 4 for the proposed climate macrostate Ω_2.

As noted earlier, to suppress the vertical movement of air into the valleys, the temperature stratification is strengthened. Since the bulk of wind energy production is in the winter, we adopt a stability condition that is representative of winter. The wintertime lapse rate (from the radiosondes) within the Whitehorse Valley is +8 K km^{-1}: the temperature profile for the Ω_2 input is set to reflect this winter condition. This temperature profile results in N = 0.026 s^{-1}, and F = 0.2 (U = 5 m s^{-1}). Variants of Ω_2 have also been investigated, and these results will also be discussed.

With the climate macrostate Ω_2 adopted to define the boundary conditions, the resulting MC2 simulation produces flow directions that generally conform better with observations at many locations. At first glance, Fig. 6 shows that the mountaintop winds blow mainly from the southwest, conforming with the boundary conditions. These mountaintop vectors line up with the observations from Flat Mountain and the Whitehorse radiosondes at 1900 m ASL (see Fig. 1). To the south of the Champagne site, the wind vectors also show southwest winds from an open valley as is expected at this location. At the grid point nearest Champagne, however, the simulation provides an erroneous northwest wind: winds in the Takhini River valley at Champagne are expected to be from west-southwest to southwest. At the two Whitehorse surface stations the simulated valley-bottom flow is generally southeast conforming to surface observations and the valley orientation. This is expected as this simulation was purposely set up with the higher pressure to the southeast, so that within the Whitehorse Valley the flow is pressure-driven from that direction.

The more important purpose of this exercise was to prevent downward momentum transfer by inducing strong stratification (i.e., F = 0.2) into the MC2 model. This is to allow a pressure-driven flow within the valley to occur uninhibited by the vertical transfers from the winds aloft when there is orographic blocking. While the Ω_1 simulation, with rather weak stratification, allowed too much downward momentum transfer with the consequence that large magnitude winds reached far down the lee slopes, the Ω_2 state appears to have suppressed this, albeit only marginally. This suppression of downward wind is evident in Fig. 7, which shows that the isentropes across the Whitehorse Valley (line A–C in Fig. 6) are relatively level and undisturbed by the mountains. The isotachs show that the downdraft does not exceed 0.15 m s^{-1}, which is an improvement over the Ω_1 simulation. The Ω_2 macrostate was also simulated with the same weak stratification as Ω_1 and the downward vertical motion in this same cross-section exceeded 0.2 m s^{-1} and was present all the way down the lee slope, in contrast to Fig. 7. In summary, Fig. 7

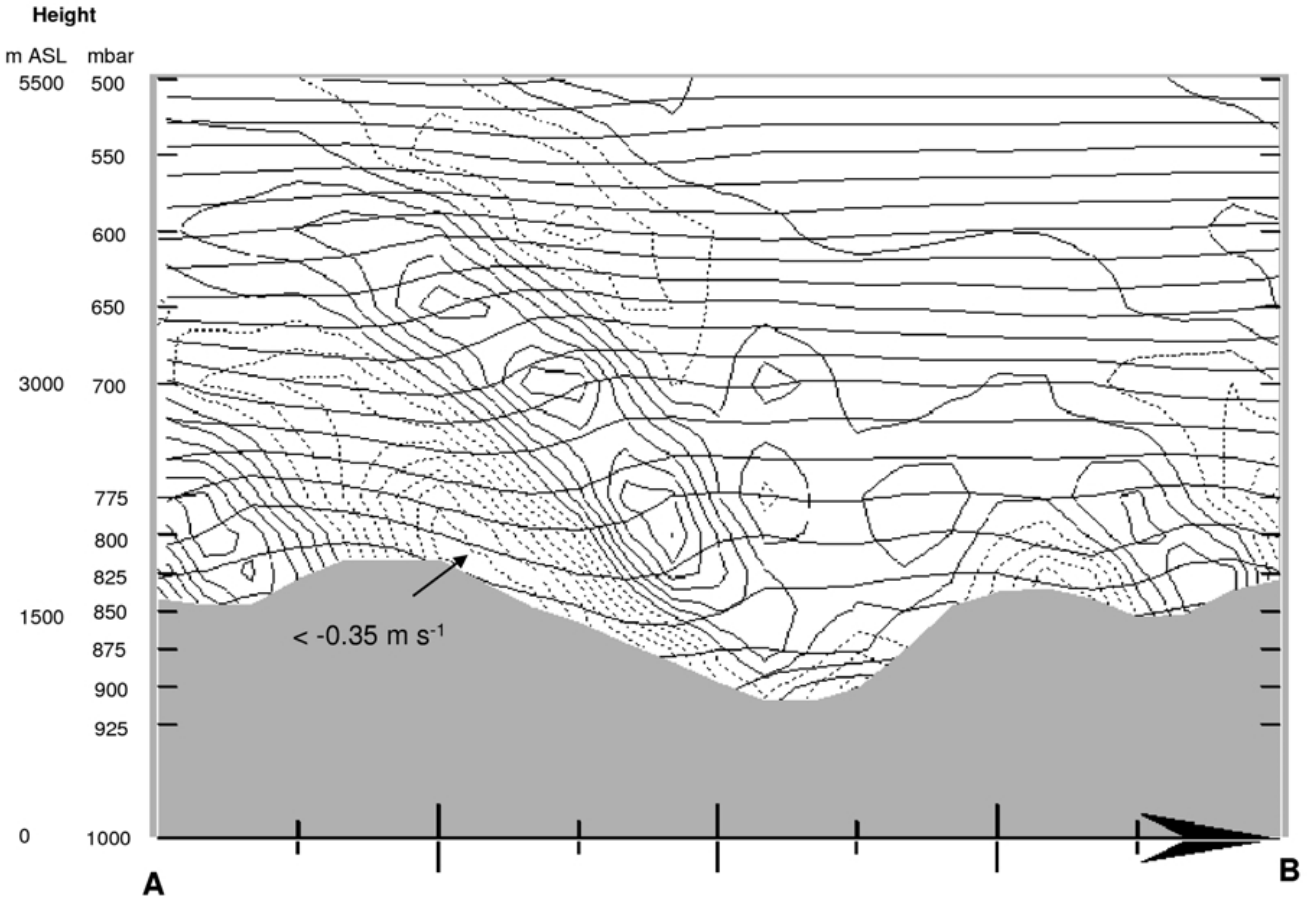

Fig. 5 Outcome of wind climate simulation based on driving MC2 with climate macrostate Ω_1 representing the Reanalysis. This is a cross-section of potential temperature and vertical velocity across the Takhini Valley, indicated by line A–B in Fig. 4. The potential temperature interval is 1 K. The vertical velocity interval is 0.05 m s^{-1} and the dashed lines are vertical velocities ≤ 0 m s^{-1}; the distance from A to B is approximately 60 km. In interpreting the pattern of the vertical motion, it is crucial to understand that the computed mean horizontal wind vector along this transect does not everywhere lie in the plane of this diagram; this is a complex 3-dimensional flow (refer to Fig. 4), not a simple uni-directional left-to-right flow.

TABLE 4. Input parameters of the climate macrostate Ω_2 used in the MC2 simulation of the Whitehorse area.

Variable	0 m	1500 m	3000 m	5500 m	Units
Wind Speed	5	5	5	5	m s^{-1}
Wind Direction	225	225	225	225	
Temperature	261	273	285	285	K
Lapse Rate	8	8	0		K km^{-1}

indicates that there should be no significant downward momentum transfer and hence there should be no high winds on leeward slopes.

But despite the deep, strong inversion and low Froude number (F = 0.2) in the Ω_2 simulation, there are still excessively large magnitude winds on the lee slope of mountains. For example, the surface wind speed at the peak of Pilot Mountain (see oval in Fig. 6) is 3.5 m s^{-1} while at the next downstream node, which is 300 m lower, it is 8.7 m s^{-1} ($w \approx -0.5$ m s^{-1}) along the same direction. This scenario of strong discrepancy in wind speed also occurred when simulated with the same Ω_2 macrostate but with lower boundary winds of 2 m s^{-1} (i.e., F = 0.08).

The massifs of Mount Arkell and Mount Granger shown in Fig. 6 act as a barrier against the southwest winds aloft and on the plateau in the lee of this range, the surface winds ought to follow along the Whitehorse Valley axis as the observations indicate (under wintertime conditions). In the simulation, however, many of the surface nodes on this plateau are southwesterly. On Mount Sumanik and Haeckel Hill for example, the surface wind directions at those nodes are unorganized while observations show clear evidence of the south-southeast winds. At the Fish station (as well as Mount Sima) the measured winds were southerly (southeasterly) under wintertime stratification but the nearest node simulated westerly winds.

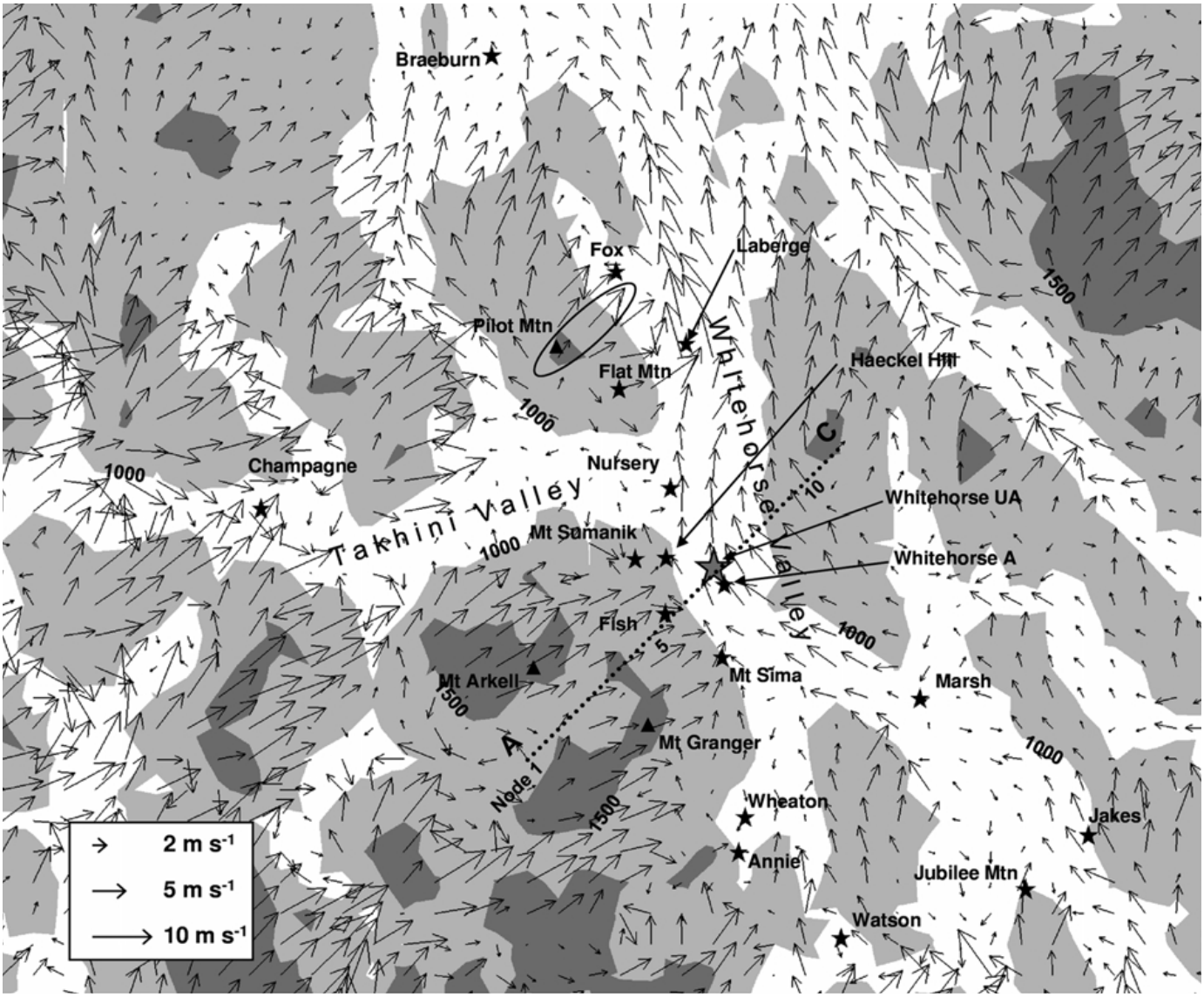

Fig. 6 As in Fig. 4 but for climate macrostate Ω_2. Note that line A-C has labelled nodes that are referred to in the discussion of Fig. 8.

To investigate this problem further a cross-section of the Whitehorse Valley with vertical profiles of horizontal wind speed is presented in Fig. 8. The cross-section runs southwest to northeast across the valley (along line A–C in Fig. 6) and follows the southwest wind direction in the model. There are several features that are apparent here and that will be addressed, starting at the upper levels. Firstly, we note that above the mountaintops (>2000 m ASL) the wind speed is generally greater than 6 m s^{-1} — a speed-up that is more than 20% higher than the imposed boundary wind speed of 5 m s^{-1}. Above the first range of mountains where nodes 1 to 4 are located there are two local wind speed maxima, or jets. The upper jet (at 4000 m ASL over node 1) is above the dashed line and appears to be a gravity wave responding to orographic disturbance. Following Pinty et al. (1995) the hydrostatic vertical wavelength $\lambda_H = 2\pi\bar{U}/N = 1.5$ km, where the ensemble mean wind speed above this area $\bar{U} = 6$ m s^{-1} and the Brunt-Väisälä frequency, calculated from the initial conditions for Ω_2, is $N = 0.026$ s^{-1}. This value for λ_H is roughly equivalent to the vertical distance between the lower and upper jet above nodes 1 to 4 and is consistent with the gravity waves produced in Pinty et al. (1995). Over nodes 3 to 5 the nose of the upper jet appears to follow the terrain-following grid, along the dashed line. Note, however, that below 3000 m ASL the atmosphere is highly stable, which might be expected to suppress vertical transport of horizontal momentum. The lower jet near the surface over the first range follows the dotted line in Fig. 8 and appears to be a localized hill speed-up. At node 3 the elevation of the jet has dropped relative to sea level but is at nearly the same height above the surface as it is at nodes 2 and 4. The lower jet disappears as the flow goes past node 5 on the downslope side of the first range.

At node 6, where the ground surface lies fully 600 m below the crest of node 4, the surface wind has become a

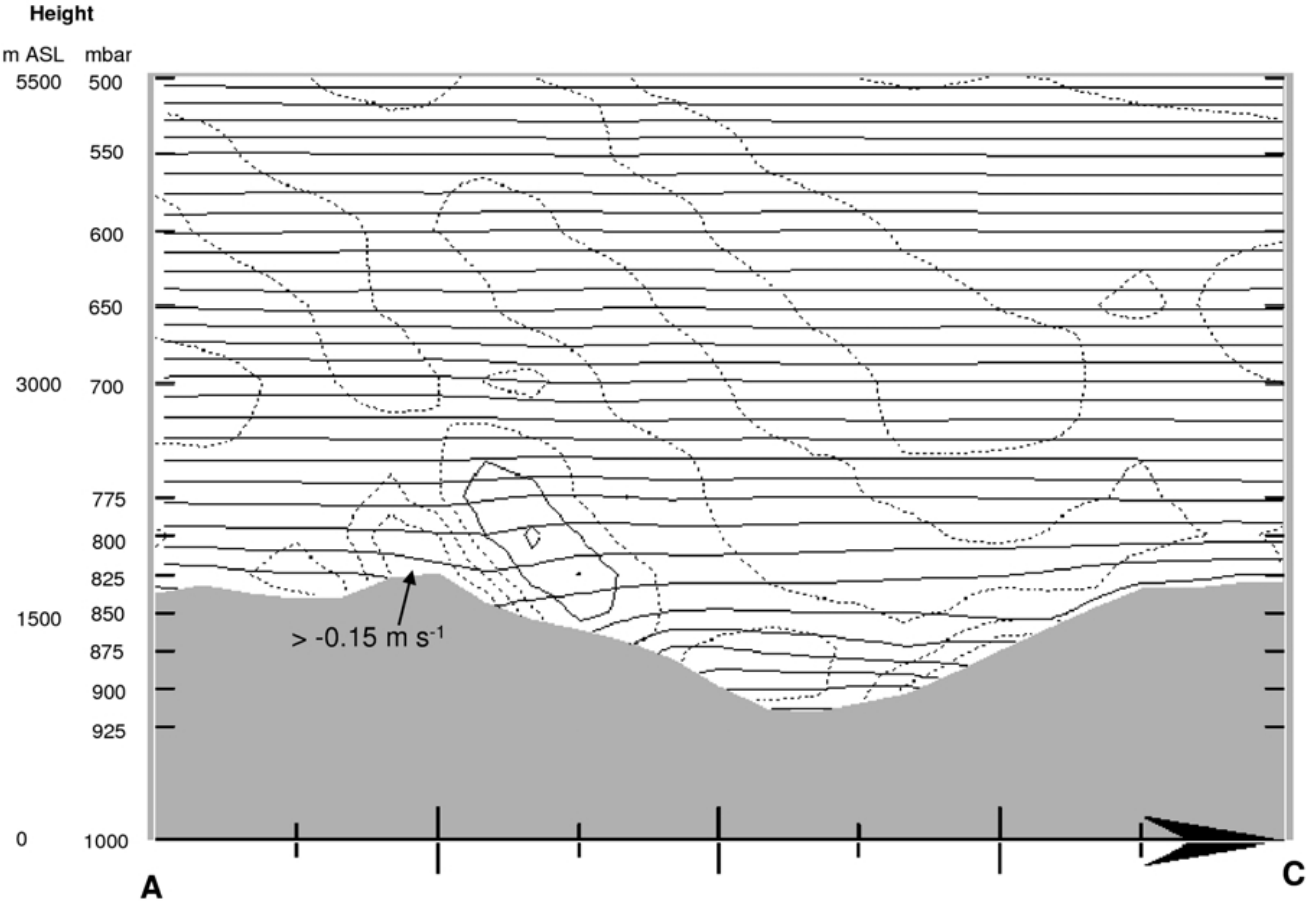

Fig. 7 As in Fig. 5 but but for climate macrostate Ω_2 and across the Whitehorse Valley, indicated by line A–C in Fig. 6. The potential temperature interval is 2 K. The vertical velocity interval is 0.05 m s^{-1} and the distance from A to C is 71 km.

southeasterly, following the valley (see Fig. 6 along line A–C). At node 6, moving up from the surface, the wind speed decreases to a local minimum not very far above ground, only to increase sharply at still higher elevations. This local minimum also appears at the nodes downstream from node 6 and is associated with a sharp veering of the wind direction and hence a separation surface, or a dividing streamline height. The thick solid line on Fig. 8 delineates a dome, whose position identifies the height at which the dividing streamline occurs. Above the dome the wind is southwesterly, and below the dome the wind direction is mostly south-southeasterly, following the valley. Within the dome a jet, having a nose at a maximum height of 220 m (third level above node 7 and 8) above the surface, is a dominant feature. Most interesting is the shape of the dome: the dome appears to be pushed up the northeast side of the valley, onto the next ridge. It would appear that the southwest wind aloft is pushing the dome up against the other side of the valley. When the simulation was repeated with a weakened stratification, the asymmetry of the dome of cold air was more marked.

Focussing our attention on the observations, the Whitehorse upper-air station is located near node 7, at the valley bottom, where the nose of the measured winter jet (500 m AGL) is twice the height of the simulated one (220 m AGL). From the radiosondes (see Fig. 1) the wind direction changes from a valley wind to a southwesterly wind at about 1700–1900 m ASL (or 1000–1200 m above the valley bottom). In the simulation, especially under a strong winter stratification, we should therefore expect that the dome of dividing streamline height should be about 1100 m above node 7 (1800 m ASL), double the height of the dome of dividing streamline height that has been simulated. Strengthening this argument, Mount Sumanik and Haeckel Hill are located near node 6 and at surface heights of 1430 and 1701 m ASL, respectively. At both surface stations predominantly south-southeast winds were measured (year-round, even under weaker stratification), and this would suggest that the height of the dome at node 6 ought to be at least 1000 m above the valley bottom (1700 m ASL). A suggested shape for this dome of dividing streamline (that is, the dividing surface as defined by observations as opposed to the simulation) is shown as a thick dash-dotted line in Fig. 8.

In concluding the discussion of Fig. 8 we note that although the inversion height (being 1500 m higher than measured) and its intensity (typical winter lapse rate) were exaggerated in the model, the wind following the Whitehorse Valley did not fill the valley as the observations suggest.

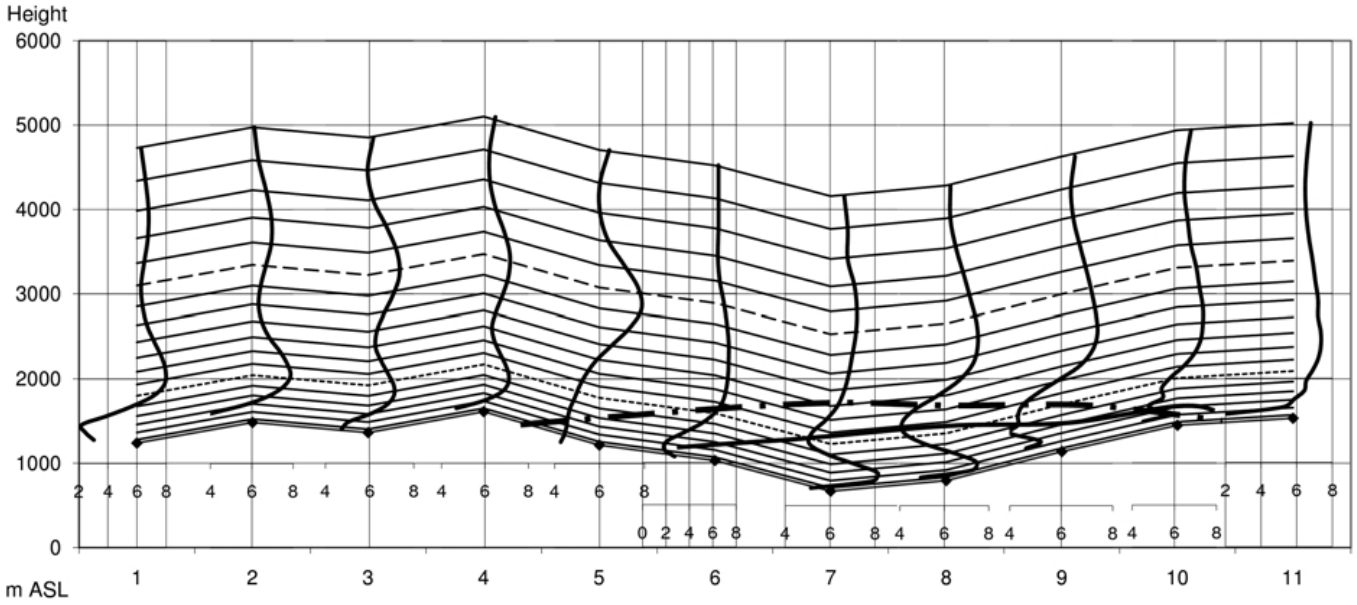

Fig. 8 Cross-section of the Whitehorse Valley running southwest to northeast, following the southwest wind direction of the Ω_2 state simulation. The abscissa corresponds to the mesoscale grid points along baseline A–C indicated in Fig. 6. These vertical profiles of horizontal wind speed flow from the southwest (±10°), except within the valley under the thick solid line delineating a dome of dividing streamline. Each profile is centred at 6 m s^{-1} through each of nodes 1 to 11. The vertical exaggeration is five times. The spacing between the nodes is 7.1 km (diagonal across 5-km square grid) and the heights of the lowest grid levels are 40, 125, 220 and 320 m AGL and increase gradually thereafter. The grid levels that are represented by a dot-dashed and a dashed line are at levels 560 and 1860 m above the model surface respectively and are for reference in the text discussion.

6 Discussion

The problems arising from the Ω_2 simulation have also appeared in comparable studies simulating valley flows with cross-winds aloft. Both Bergstrom and Juuso (2006) and Gross and Wippermann (1987) simulated valley jets that were concentrated on the downwind side of a valley relative to the crossing wind aloft and under relatively stable conditions. Vogel et al. (1986) also carried out simulations that showed channelling with a jet maximum very close to the valley bottom and away (downstream towards the east side of the valley) from the main flow aloft in the Upper-Rhine Valley. But according to Vogel et al. (1986) when the measured wind aloft was from the west crossing the Upper-Rhine Valley the observed channelling could be found on the west side of the valley, opposite to their simulated valley wind. This was observed in a field experiment (Fiedler and Prenosil, 1980) in which nine weather balloon stations were placed across the Upper-Rhine Valley. As the winds aloft increased, a valley jet intensified towards the middle (horizontally and vertically) of the valley and channelling spread widely and evenly across the valley. Vogel et al. (1986) also showed that valley channelling could reach hundreds of metres above the mountaintops bordering the valley on a typical September day (our calculations from their study showed, surprisingly, that $F \simeq 1.5 - 2$). Vogel et al. (1986) have shown, and this is also demonstrated in our study, that the simulated valley wind stream is pushed further downward and downstream relative to the winds aloft than the observations of the same circumstance suggest.

One of the features these models have in common with the MC2 model is that they use a terrain-following (or σ-) coordinate system. The coordinate transformation splits the horizontal pressure gradient into the sum of two terms, one of which involves the *vertical* pressure gradient. Near steep slopes these terms become large and a small error in computing either term can result in a large error in the total pressure gradient force (Haney, 1991). Janjic (1989) tested a σ-coordinate system with a single mountain in the middle of a horizontally homogenous atmosphere at rest. He found significant errors in the pressure gradient force that corresponded with the presence of an imposed temperature inversion. These errors were, however, restricted to points over the sloping terrain.

These errors were less serious in low resolution modelling studies which had been provided with a highly smoothed topographic field. However, as the grid is refined regions of (locally) steep slope occur, such that the slope-induced errors in the representation of the horizontal pressure gradient can no longer be ignored (see Mesinger (2003) for a detailed discussion). Steppeler et al. (2002) note that for better accuracy in terrain-following coordinates one should require $\delta h < \delta z$, where δh is the change of orographic height from one horizontal grid point to the next, and δz is the vertical grid interval. Whereas in the Whitehorse domain $\delta z = 40$, 85 and 95 m in the lowest three grid cells, δh can reach values that exceed 500 m on the steeper slopes such as those at Pilot Mountain. Walko et al. (1995) suggest a rule of thumb that δh should not exceed 3 to 5 times δz, a criterion that, in the present

simulations, was violated on many slopes on the Whitehorse domain.

For finer horizontal grids Steppeler et al. (2002) proposed a z-coordinate system with an approximate finite-volume technique at the orographic boundary. Steppeler et al. (2006) tested this with measurable success in simulations of rain in the steep mountains of Europe. Although their focus was on predicting precipitation they found reduced velocity errors near mountain slopes when compared to the terrain-following system. Even though they were satisfied with the simulated mountain-lee winds compared to terrain-following simulations, they could not confirm the results due to a lack of stations in the domain of interest.

The discussions in this section along with those based on Fig. 8 suggest that when simulating regions of steep terrain at high resolution, such as the Yukon, accuracy is limited by the use of the terrain-following coordinate. To progress, one might need to revert to a basic z-coordinate system. A proposed method for the MC2 model is a grid cell blocking approach to implement the lower boundary condition to the three-dimensional flow around obstacles. This is currently being tested in experimental versions of the MC2 model (P. Pellerin, personal communication, 2008). Eventually, this scheme will need to be tested (as here against observations) to check whether it represents a further improvement of the AnemoScope method in complex terrain.

Based on the present study, can one attempt to generalize the main findings to eventually improve AnemoScope and future versions of the Canadian Wind Atlas? To a limited degree, yes.

a) Only Reanalysis data from levels well above the mountaintops should be used to initialize the EOLE mode of the MC2 model.
b) The option of having the topography of interest (when using the MC2 model in the EOLE mode) surrounded by a high plain, in lieu of the *sea-level* plain currently used, would be useful.
c) Care must be taken in selecting the representative temperature profile, at least in the lower atmosphere, due to the large effect stratification has on the resulting airflow.
d) Assuming that the low-level stratification in the Reanalysis data is representative of that measured by the radiosondes, then one should modify the classification scheme used to define the climate macroscopic states such that the binning is based on the geostrophic wind vector (as before) and the strength of the thermal stratification, perhaps in the form of a Froude number. This last parameter could replace (or be combined with) the sign of the geostrophic wind shear currently used.

7 Conclusions

Two simplified climate states were simulated using the MC2 model in the steep mountainous terrain of the Whitehorse region. The first climate state representing the Reanalysis was shown to result in erroneous wind directions in all but the Whitehorse Valley where the upper-air station is located. This was primarily due to the incorrect assumption that the winds within the domain of the orographic influences are geostrophic and were incorrectly used to set the pressure gradients in the model.

A better simulation resulted when using (as a boundary condition) a height constant geostrophic wind speed and direction that is associated with the Reanalysis (and Whitehorse radiosondes) above the mountaintops. In this case the wind vectors conformed better to observations. In conjunction with this step an attempt to reduce the downward momentum transfer was made by adjusting the temperature profile to a highly stable state that is typical of wintertime conditions. Despite the imposed stratification there remained substantially high magnitude winds on the steep mountain lee slopes that are suspected to have been caused by errors due to a terrain-following grid structure.

To improve upon the MC2 simulation in deep mountainous terrain the main recommendations are to consider a basic z-coordinate grid for the model, to reprocess the Reanalysis data by ignoring the statistics that are affected by the orography and project down geostrophic winds from aloft, and to put more care into temperature profile selection in the lower atmosphere.

Acknowledgements

The first author would like to acknowledge the following: Environment Canada for scholarship funding towards this study; the Natural Sciences and Engineering Council (NSERC) and the Northern Scientific Training Program/Canadian Circumpolar Institute (NSTP/CCI) for scholarship funding; NCEP/NCAR for the Reanalysis data, and the radiosonde observations (RAOBS) data centers; the Yukon Government (Yukon Energy, Community Services and Wildland Fire Management); and Sally Wright for her love and support throughout this study.

We would also like to acknowledge Herbert Wahl, a retired Yukon meteorologist who passed away recently. This study is dedicated to the memory of Doug B. Craig, an inspiring and pioneering wind prospector in the Yukon.

References

BERGSTRÖM, H. and N. JUUSO. 2006. A study of valley winds using the MIUU meso-scale model. *Wind Energy*, **9**(1-2): 109–129.

CHC&EC (CANADIAN HYDRAULICS CENTRE AND ENVIRONMENT CANADA). 2006. Anemoscope Wind Energy Simulation and Mapping User's Guide. Canadian Hydraulics Centre and Environment Canada.

FIEDLER, F. and T. PRENOSIL. 1980. Das MESOKLIP-experiment, mesoskaliges klimaprogramm in oberrheintal. Wiss. Ber. Meteorol. Inst. Univ. Karlsruhe, Tech. rep. 1, 107 pp.

FREY-BUNESS, A.; D. HEIMANN and R. SAUSEN. 1995. A statistical-dynamical downscaling procedure for global climate simulation. *Theor. Appl.*

Climatol. **50**: 117–131.

GIRARD, C.; R. BENOIT and M. DESGAGNÉ. 2005. Finescale topography and the MC2 dynamics kernel. *Mon. Weather Rev*. **133**(6): 1463–1477.

GROSS, G. and F. WIPPERMANN. 1987. Channeling and countercurrent in the upper Rhine Valley: Numerical simulations. *J. Clim. Appl. Meteorol.* **26**(10): 1293–1304.

HANEY, R. L. 1991. On the pressure gradient force over steep topography in sigma coordinate ocean models. *J. Phys. Oceanogr.* **21**: 610–619.

JANJIC, Z. I. 1989. On the pressure gradient force error in σ-coordinate spectral models. *Mon. Weather Rev.* 117: 2285–2292.

KALNAY, E.; M. KANAMITSU, R. KISTLER, W. COLLINS, D. DEAVEN, L. GANDIN, M. IREDELL, S. SAHA, G. WHITE, J. WOOLLEN, Y. ZHU, A. LEETMAA, B. REYNOLDS, M. CHELLIAH, W. EBISUZAKI, W. HIGGINS, J. JANOWIAK, K. C. MO, C. ROPELEWSKI, J. WANG, R. JENNE and D. JOSEPH. 1996. The NCEP/NCAR 40-year Reanalysis project. *Bull. Am. Meteorol. Soc.* **77**: 437–471.

MESINGER, F. 2003. The steepness limit to validity of approximation to pressure gradient force: Any signs of an impact. *In*: Preprints 20th Conf. on Weather Analysis and forecasting/16th Conf. on Numerical Weather Prediction, paper P1.19, Seattle WA USA.

PINARD, J.-P. 2005. Wind climate of the mountainous Yukon. *In*: New Northern Lights: Graduate Research on Circumpolar Studies from the University of Alberta. Canadian Circumpolar Institute.

PINARD, J.-P. 2007. Wind climate of the Whitehorse area. *Arctic*, **60**(3): 227–237.

PINARD, J.-P.; R. BENOIT and W. YU. 2005. A WEST wind climate simulation of the mountainous Yukon. ATMOSPHERE-OCEAN, **43**(3): 259–282.

PINTY, J.-P.; R. BENOIT, E. RICHARD and R. LAPRISE. 1995. Simple tests of a semi-implicit semi-Lagrangian model on 2D mountain wave problems. *Mon. Weather Rev.* **123**: 3042–3058.

SMEDMAN, A.-S. and H. BERGSTRÖM. 1995. An experimental study of stably stratified flow in the lee of high mountains. *Mon. Weather Rev.* **123**: 2319–2333.

STEPPELER, J.; H. W. BITZER, M. MINOTTE and L. BONAVENTURA. 2002. Nonhydrostatic atmospheric modeling using a z-coordinate representation. *Mon. Weather Rev.* **130**: 2143–2149.

STEPPELER, J.; U. SCHÄTTLER, P. PROHL, U. DAMRATH, H. W. BITZER, Z. JANJIC, U. GJERTSEN, L. TORRISI, J. PARFINIEVICA and E. AVGOUSTOGLOU. 2006. Prediction of clouds and rain using a z-coordinate nonhydrostatic model. *Mon. Weather Rev.* **134**: 3625–3643.

TANGUAY, M.; A. ROBERT and R. LAPRISE. 1990. A semi-implicit semi-Lagrangian fully compressible regional forecast model. *Mon. Weather Rev.* **118**: 1970–1980.

THOMAS, S.; C. GIRARD, R. BENOIT, M. DESGAGNE and P. PELLERIN. 1998. A new adiabatic kernel for the MC2 model. ATMOSPHERE-OCEAN, **36**: 241–270.

VOGEL, B.; G. GROSS and F. WIPPERMANN. 1986. MESOKLIP (first special observation period): Observations and numerical simulation a comparison. *Boundary-Layer Meteorol.* **35**: 83–102.

WALKO, R. L.; C. J. TREMBACK and R. F. A. HERTENSTEIN. 1995. RAMS the regional atmospheric modeling system, version 3b, user's guide. Tech. rep., ASTER Division, Mission Research Corporation, Fort Collins, CO.

WALMSLEY, J.; D. WOOLRIDGE and J. SALMON. 1990. MS-micro/3 user's guide. Tech. Rep. ARD-90-008, Atmospheric Environment Service, 85 pp.

WHITEMAN, C. D. 2000. Mountain Meteorology. Oxford University Press.

YU, W.; R. BENOIT, C. GIRARD, A. GLAZER, D. LEMARQUIS, J. R. SALMON and J. P. PINARD. 2006. Wind energy simulation toolkit (WEST): A wind mapping system for use by the wind-energy industry. *Wind Engin.* **30**(1): 15–33.